J. Hydrol. Hydromech., 72, 2024, 4, 447–465
https://doi.org/10.2478/johh-2024-0027

sciendo Journal of Hydrology and Hydromechanics Institute of Hydrology SAS

Spatial patterns of evaporation in a small catchment

Patrick Hogan[1], Borbala Szeles[1*], Gerhard Rab[1], Markus Oismüller[2], Lovrenc Pavlin[3], Juraj Parajka[1], Peter Strauss[4], Günter Blöschl[1]

[1] Institute of Hydraulic Engineering and Water Resources Management, Faculty of Civil Engineering, Vienna University of Technology, Karlsplatz 13 E222/2, 1040 Vienna, Austria.
[2] Federal Government of Lower Austria, Landhausplatz 1, 3109 St. Pölten, Austria.
[3] Austrian Federal Ministry of Agriculture, Forestry, Regions and Water Management, Department for Water Balance, Stubenring 1, 1010 Vienna, Austria.
[4] Federal Agency of Water Management, Institute for Land and Water Management Research, Pollnbergstraße 1, 3252 Petzenkirchen Petzenkirchen, Austria.
[*] Corresponding author. Tel.: +43 (0)1 58801-22335. E-mail: szeles@hydro.tuwien.ac.at

Abstract: In this study a network of three eddy covariance stations rotated between five measurement sites is used to measure evaporation (E) within the Hydrological Open Air Laboratory (HOAL) in Petzenkirchen, Austria for 8 years. Discharge measurements at the tributaries and outlet of the main catchment allow for E to be estimated for 6 subcatchments using the water balance method. Year to year variability in monthly E measured by the eddy covariance stations is found to be driven primarily by net radiation and temperature and annual E by net radiation. Year to year variability in the water balance-based E estimate was driven by precipitation. The two methods are found to be consistent, when storage and leakage are accounted for. Daily and seasonal patterns can be seen resulting from the agricultural land use cycle, due to the variations in land cover during the growing season.

Keywords: Evapotranspiration; Water balance; Agricultural catchment; Experimental catchment.

INTRODUCTION

Evaporation (*E*) is one of the most important processes in describing the surface- atmosphere interaction as it connects the energy and water balances. Knowledge of the spatial variations in *E* is important for agricultural water use and conservation at a local level, and for improving estimates of regional water balances at larger scales (Bastiaanssen et al., 2005).

Research on *E* can be roughly divided into five spatial scales of study: global and continental scale, regional scale, meso-scale (~20–500 km^2), field scale and leaf scale. Each scale requires different methodology in order to estimate *E*, with significant differences in the spatial and temporal limitations and accuracy between the methods. At the regional and meso scales *E* may be estimated using remote-sensing-based models based on thermal or visible imagery supported by ground observations (Eswar et al., 2017; Ruhoff et al., 2013), while at the field scale *E* can be measured directly, however the heterogeneity of the terrain and vegetation imposes a spatial limitation on the estimates (Shimizu et al., 2015). In order to bridge the gap between the meso-scale and the field scale this heterogeneity must be accounted for. A combination of ground-based measurement systems and remote sensing imagery or upscaling has frequently been used. The SMACEX and BEAREX08 experiments used eddy covariance towers and remote sensing temperature and vegetation products to investigate *E* in agricultural catchments over short term periods, finding spatial and temporal differences between the different crop types (Anderson et al., 2012; Kustas et al., 2005). Prueger et al. (2005) measured spatial and temporal variations due to differences in canopy cover and soil moisture between maize and soy crops using tower and aircraft eddy covariance measurements, with the Bowen Ratio of maize being twice that of soy at the start of the experiment before converging due to increased precipitation (*P*) and leaf area as the crops approached maturity. Hssaine et al. (2021) estimated large spatial variations in latent heat flux (*LE*) using soil moisture remote sensing products in combination with Landsat imagery, with differences of up to 500 Wm^{-2} between vegetated and bare fields. Armstrong et al. (2019) used thermal and visible images from an unmanned aerial vehicle and eddy covariance measurements to estimate *E* according to net radiation (*Rn*) across a mixed wetland/agricultural area for one day, reporting lower rates of mean daily *E* where vegetation was less dense and higher rates associated with densely vegetated areas and wetland fringes. Long term studies of the spatial differences in *E* at the small catchment scale are however lacking.

The catchment water balance method can also be used to estimate interannual spatial and temporal variability in *E* at various scales. While good convergence of the catchment water balance and eddy covariance methods in smaller catchments has been reported (Denager et al., 2020; Wilson et al., 2001), considerable variability may be found on a year-to-year basis with Scott (2010) reporting a range of –10 to 17%. In addition, storage and leakage might become non-negligible in smaller catchments with Tie et al. (2018) reporting water balance-based estimates of *E* over 100 mm higher compared to eddy covariance-based, which they postulated might be due to subsurface runoff. At the small catchment scale the water balance is evaluated over the entire catchment area, however the gauging of tributaries could be used to provide spatial information on the variability of *E* on a subcatchment basis.

To utilise information on the spatial patterns of *E* the spatial and temporal drivers must also be known. These can vary between climate and ecosystem. At regional scales in arid and semi-arid areas land use (Bouwer et al., 2008) and *P* (Valayamkunnath et al., 2018) are identified as key spatial and temporal drivers, while in humid areas the drivers of the variability are more complex, with wind speed, humidity, precipitation, soil moisture, temperature, solar radiation and land

use (Jiang et al., 2020; Liang et al., 2011; Xu et al., 2006; Zhang et al., 2010) all being variously reported as responsible for variations in *E*. Less is known about the drivers at the small catchment scale, as intensive measurement campaigns tend to be of short duration. Hatfield and Prueger (2011) found that short term spatial variation among different crop fields could be attributed to variations in solar radiation due to cloud cover, precipitation and soil water availability due to soil type and rooting depth.

Most studies investigating the spatial patterns of *E* tend to be of limited duration or temporal resolution due to the high instrumentation requirements or limited to regions with good climatic conditions for remote sensing imagery with few long-term studies available. Accordingly, the objectives of this paper are to investigate (1) the spatial patterns of evaporation and (2) their drivers, in a small agricultural catchment at daily to yearly timescales. The work is based on 8 years of eddy covariance measurements and water balance-based estimates using measurements made at the Hydrological Open Air Laboratory (HOAL) in Petzenkirchen, Austria.

MATERIALS AND METHODS

Experimental Site

The HOAL is located in the western part of Lower Austria (15° 9' E, 48° 8' N) (Blöschl et al., 2016). It is an agricultural catchment, 66 ha in size with the majority of the land being used for crops (87%), with a smaller amount covered by forest (6%) and the remainder consisting of meadows (5%) and paved surfaces (2%) (Figure 1). The dominant soil types in the catchment are Cambisols (57%), Kolluvisols (16%), Planosols (21%) and Gleysols (6%) next to the stream (Blöschl et al., 2016). The catchment altitude ranges from 268 m to 323 m with a mean slope of 8%.

The crops grown are predominantly corn, winter wheat and rapeseed. Figure 2 shows the land use in each field from 2013-2020 and the locations of the eddy covariance stations. Winter crops are generally planted in late October/ November and harvested in July. Maize crops are sown in April and harvested in September/ early October depending on the weather conditions and the resulting moisture content of the plants. Table 1 shows the planting and harvesting dates for fields in the immediate locality of the eddy covariance stations.

The mean annual temperature (*T*) at the catchment ranged from 9.4–10.7 °C over the course of the measurements with an average of 10.1 °C. Annual *Rn* varied from 1.01–1.23 MW/m^2 with an average of 1.14 MW/m^2. There was a positive trend towards warmer and sunnier summers with 2013 and 2014 recording below average values for the summer months (Figure 3).

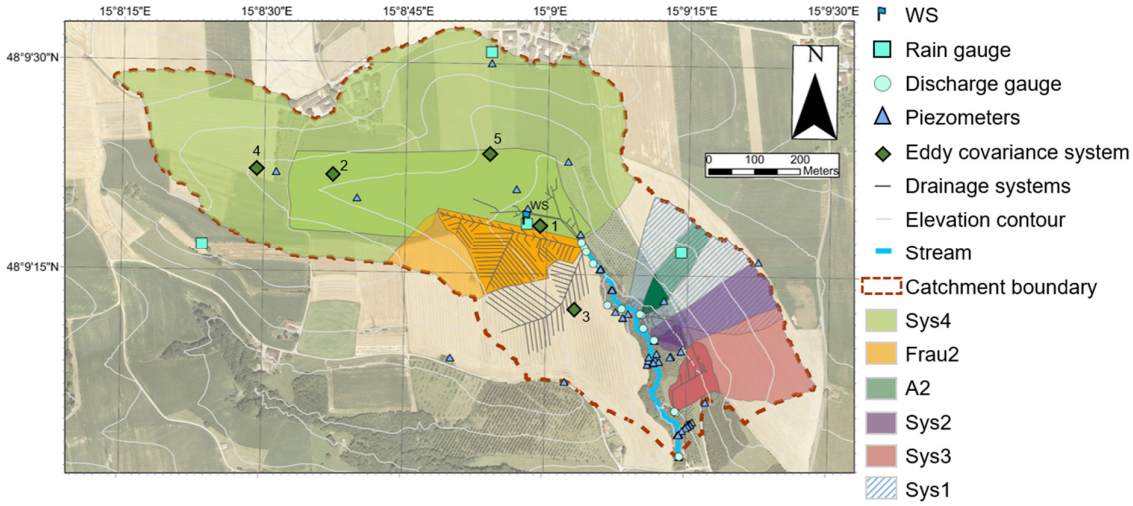

Fig. 1. Map of the catchment and instrumentation network. The locations of the temporary eddy covariance stations are numbered 1 – 5 according to Table 2, with the central weather station marked as WS. Subcatchment areas are displayed as shaded areas, with maximum and minimum areas shown for each subcatchment. Minimum areas are highlighted as a darker shade. Maximum subcatchment areas are delineated according to topography, while minimum areas exclude areas which may be affected by local drainage networks.

Table 1. Planting and harvesting dates for the winter (winter wheat, winter barley and rapeseed) and summer crops (maize) at adjacent to mobile eddy covariance device locations (Figure 2).

Year	Winter crop sowing date	Winter crop harvest date	Summer crop sowing date	Summer crop harvest date
2014	22nd Aug. 2013	1st Jul.	4th Apr.	30 Sep.
2015	24th Sep. 2014	10th Jul.	15–24th Apr.	7–15th Sep.
2016	29th Aug. 2015	23rd Jul.	25–27th Apr.	30th Sep.–14th Oct.
2017	25th Aug. 2016	14th Jul.	22nd Apr.	25th Oct.
2018	–	–	20th Apr.	1st Oct./25th Sep.
2019	27th Sep. 2018	30th Jun.	16th Apr.	27th Sep.
2020	16th Oct. 2019	1st Jul.	11th Apr.	24th Sep.

Table 2. Installation details of eddy covariance sensors (see Figure 1 for locations).

From	To	Location (Figure 1)	Device type	Installation height (m)	Direction (°)
1/1/2013	26/8/2015	1	IRGASON	2.7	270
26/8/2015	31/12/2020	1	EC155	2.7	270
1/1/2014	1/1/2015	2	EC155	2.7	270
1/1/2015	26/8/2015	3	EC155	2.2	270
26/8/2015	4/8/2016	3	IRGASON	2.2	270
1/6/2015	31/12/2020	4	IRGASON	3.5	270
4/8/2016	31/12/2020	5	IRGASON	4.5	180

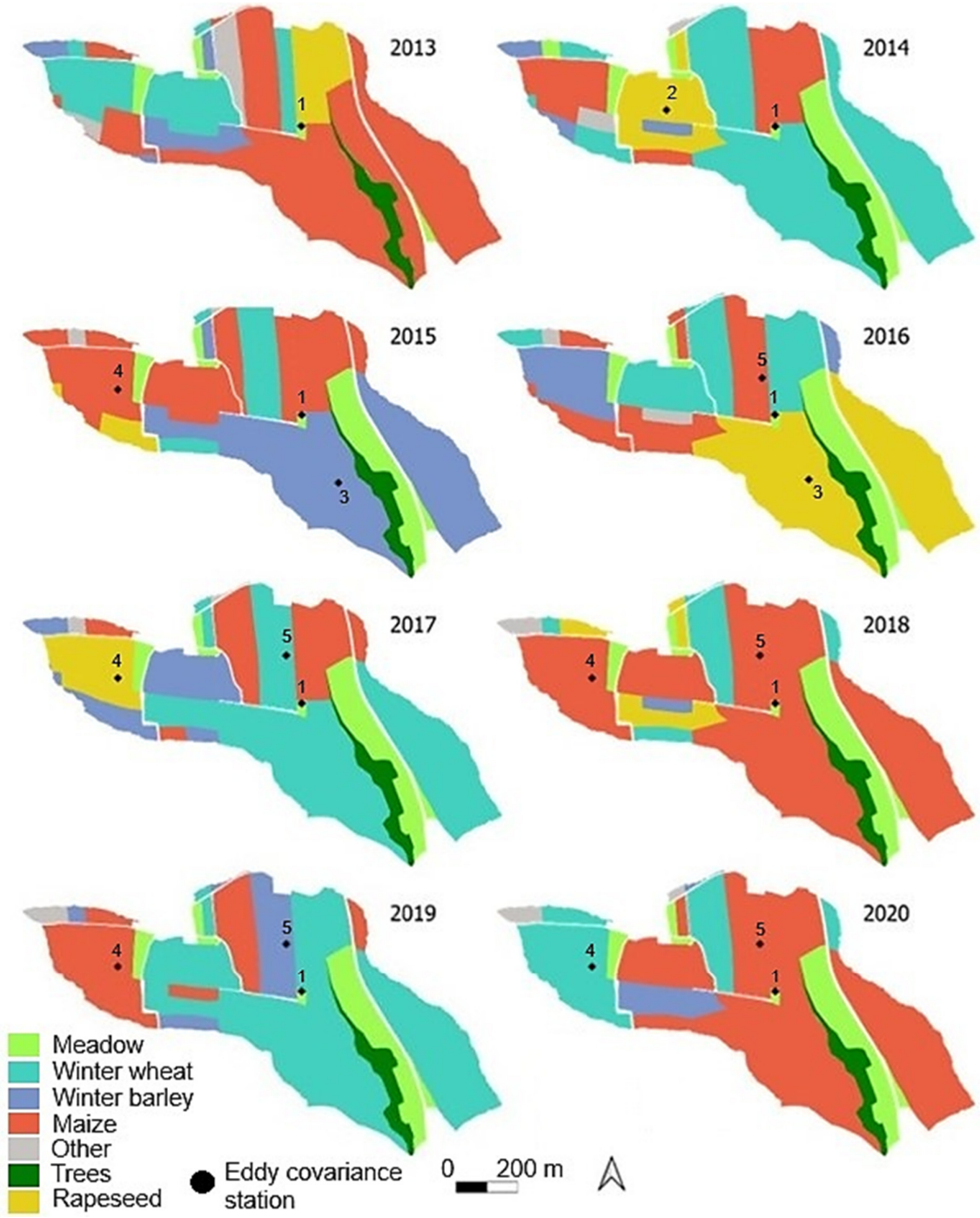

Fig. 2. Main crop type for each field from 2013–2020. Locations of eddy covariance stations marked with black diamonds.

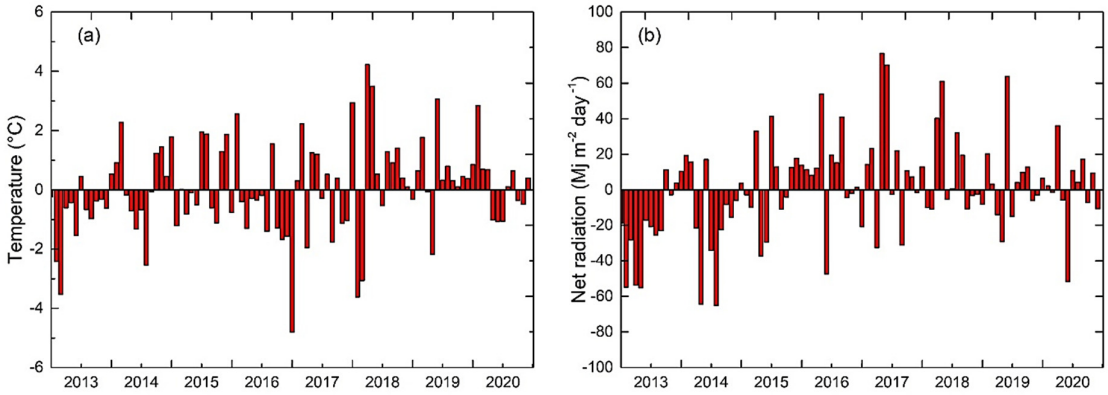

Fig. 3. Monthly values of the (a) deviation from the average monthly temperature, and (b) deviation from the average monthly net radiation sum.

Instrumentation and measurements

The weather station at the centre of the catchment was equipped at 2 m height with temperature and humidity sensors (HMP-155, Vaisala), a wind sensor (Windsonic 232, Gill), and a 4-component net radiation sensor (CNR-4 Kipp and Zonen). In 2013 and 2015–2020 two soil heat flux plates (HMP01, Huskeflux) were installed at a depth of 30 cm, with the soil heat flux at the surface calculated according to the calorimetric method described in Mauder et al. (2006) using a profile of soil temperature (T107, Campbell Scientific) and soil moisture (Spade-TDT, Jülich) probes installed at 30 cm, 20 cm, 10 cm and 5 cm depths. The meteorological data was measured at 1-5 second frequency and 30-minute averages were calculated and stored on a CR3000 datalogger (Campbell Scientific).

E was measured at the catchment from 2013 using a network of 3 eddy covariance devices (Figure 1); two open-path systems (IRGASON, Campbell Scientific) and one closed-path (EC-155, Campbell Scientific). At the weather station an IRGASON (Campbell Scientific) open path eddy covariance sensor was installed on a 10 m tower at a height of 2.7 m. This was then replaced on the 26/8/2015 by the closed path eddy covariance sensor. The two other eddy covariance devices were installed at various locations on tripods (Figure 4) within the catchment according to the agricultural crop rotation (Table 2). In 2014 and the first half of 2015 the soil heat flux plates were installed alongside the closed path device at locations 2 and 3 (Figure 1). The installation heights of the devices were adjusted in relation to the surrounding vegetation, to control the footprint size.

Measurements of the three-dimensional wind speed and water vapor density (IRGASON) /water vapor mixing ratio (EC155) were made at 10 Hz and saved on a CR3000 datalogger (Campbell Scientific) using a CF card. From 2013-September 2015 the sensible (*H*) and latent heat fluxes (*LE*) were processed offline using the Eddy-Covariance Software TK3 from Bayreuth University (Mauder and Foken, 2015). After September 2015 the fluxes were calculated online at the dataloggers using the EasyFlux software from Campbell Scientific. This was done to reduce data loss due to problems with the CF storage cards malfunctioning at the dataloggers; as the processed fluxes have a much lower storage space requirement than the raw data, they could additionally be saved in the datalogger memory. Measurements with a low signal strength or spikes as flagged by the device were removed by the software before calculating the covariances. The covariances were calculated for a 30-minute averaging period. During the processing of the fluxes a number of corrections were applied to the calculated covariances:

(1) A double rotation of the coordinate system
(2) The Moore correction for low-frequency response (Moore, 1986)
(3) The sonic air temperature correction for *H* (Schotanus et al., 1983)
(4) The WPL correction for air density fluctuations (Webb et al., 1980)

The processed fluxes were then controlled for implausible values ($-30 > LE > 500$, $-100 > H > 700$) and the *LE* was converted to evaporation rates. When no data was available due to a failure of the device, 30-minute daytime gaps were filled using *Rn* when available. From the last good quality *LE* value, the *LE/Rn* ratio was calculated and used to fill *LE*. For calculating monthly and annual balances daily gaps were filled using the FAO-56 Penman Monteith method (Allen et al., 1998).

The *LE* data from the closed-path sensor was found to be unreliable, as the optical lenses of the infra-red gas sensor were quickly obscured by dust particles not filtered by the device intake, resulting in a non-linear decrease in signal strength of the water vapor mixing ratio which could not be corrected later. The *LE* from this sensor was instead calculated from the energy balance using *H* (1)

$$Rn - G = LE + H \quad (1)$$

In 2014 and the first half of 2015 the soil heat flux plates were therefore installed alongside the closed path device at locations 2 and 3 (Figure 1), to provide a measurement for the soil heat flux (*G*). To take into account the energy balance closure, all components of the energy balance were measured at the site in 2013 and the measured closure (26%) was subtracted from the available energy (*Rn* – *G*).

To estimate the reliability of the eddy covariance measurements the energy balance closure was analysed. By measuring all the components of (1) and performing a linear regression of the fluxes, the extent of the closure of the energy balance could be estimated. This was performed for the calendar year 2013 where all the components were measured at the central weather station, with the turbulent fluxes (*LE* + *H*) measured by the IRGASON eddy covariance device and the available energy (*Rn* – *G*) by the CNR4 device and the soil heat flux plates (Figure 5a). The regression line slope of 0.74 ($R^2 = 0.93$) fell within the commonly reported range of 10–30% missing energy (Eshonkulov et al., 2019; Leuning et al., 2012; Wilson et al., 2002). The analysis was performed for one entire year to avoid a seasonal bias, however, the possibility of differences on an inter-annual scale could not be excluded. As the soil heat flux plates

Fig. 4. Eddy covariance system (IRGASON) mounted on a 2.5 m tripod.

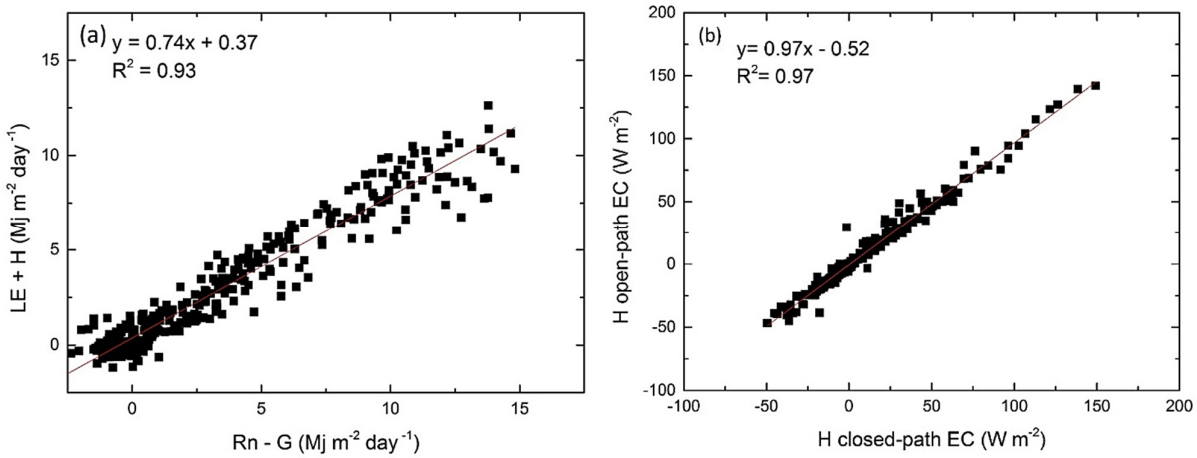

Fig. 5. Energy balance closure for the year 2013 (a) and comparison of sensible heat flux from the open- and closed-path eddy-covariance devices (b).

were removed in 2014, it was not possible to extend the analysis for longer than one year. Various reasons for the commonly reported imbalance have been put forward (Foken, 2008; Leuning et al., 2012; Mauder et al., 2006), e.g., errors in the eddy covariance measurements and flux corrections, neglection of the heat storage in the air, underestimation of the soil heat flux as the storage in the final centimetres cannot be accurately measured, secondary circulations. Imukova et al. (2016) found for an agricultural catchment at a similar latitude and climatological conditions (mean annual temperature between 9 and 10 °C and precipitation between 730 and 830 mm) that *LE* was not a major component of the energy balance gap. It is possible to force the energy balance closed by attributing the missing energy to the sensible and latent heat fluxes, however, considerable uncertainty remains as to the suitability of the various closure models. As it is not possible to attribute the lack of closure at the catchment to any definite cause and considering the results of Imukova et al. (2016), the latent and sensible heat fluxes were not corrected to close the energy balance in this study, as in other similar studies (Tie et al., 2018; Zhang et al., 2014). To check the appropriateness of using the energy balance to calculate *LE* using *H* and closure factor for the closed path eddy covariance device, the *LE* measured at the central tower was compared with the *LE* calculated using *H* measured by the same device for 2013. The two methods compared well with yearly totals of *E* of 391 mm and 374 mm for the measured and calculated *LE* respectively. The difference between the monthly totals of *E* varied between –13.2 and 13.4%, and –8.6 and 9.1 mm for the period April–September. To determine differences between the different types of eddy covariance device, an open-path and the closed-path device were installed together at the tower for one week in March 2015 and the calculated *H* fluxes compared. Minimal difference was found between the two devices, with a scatterplot comparison giving a R^2 coefficient of 0.97 and a slope of 0.97 (Figure 5b).

The measurements from the individual eddy covariance stations were upscaled to the catchment area according to the land use corresponding to each sensor. We assumed that local differences in soil moisture between the different fields were small so that *E* measured at one land use was valid for all similar fields in the catchment. Further, we assumed that the riparian zone had a *E* rate of 1.1 times the grassland meadow at the weather station due to its predominantly forested vegetation with wet understory cover, estimated from the modified crop

coefficient for tree plantations from Fischer et al. (2011) and the crop coefficient for small vegetation wetland from Allen et al. (1998).

In this study precipitation time series *(P*) observed by four weighing rain gauges distributed throughout the catchment for the period 2013–2020 were used. For the water balance calculations, the one-minute observations of the four sensors were averaged and summed for every hour. Runoff time series were observed at the catchment outlet and at 6 tributaries. Runoff was monitored at the outlet of the catchment (MW) by a calibrated H-flume with a pressure transducer, while at the inlet (Sys4), the tile drainage systems (Frau1 and Sys2), the deep aquifer tile drain (Sys1), the tile drain/wetland (Sys3) and at a wetland (A2) H-flumes and pressure transducers were used to monitor the flow. In 2019 the flumes at the tributaries were upgraded. Details on the sensors are found in Blöschl et al. (2016), while the runoff generation mechanisms were described by Exner-Kittridge et al. (2016) and Széles et al. (2018). For the water balance calculations, the one-minute observations were averaged for every hour and scaled by the (sub)catchment area. As there is some uncertainty regarding the true size of certain subcatchments, minimum and maximum areas, referred to as *min* and *max*, have been used in this study for these subcatchments (see Figure 1).

Soil moisture (*SM*) was measured using a soil moisture sensor (Spade-TDT, Jülich) located at the weather station with sensors located at 5, 10, 20 and 50 cm depths below the ground surface. The groundwater level in the riparian zone along the stream was monitored using 19 piezometers, with a temporal resolution of five minutes. As the groundwater levels in the riparian zone close to the stream were generally higher compared to the catchment average groundwater levels which might introduce a bias, 8 piezometers were installed in deep boreholes further away from the stream on the hillslopes and valley bottom of the catchment in 2017. A good agreement was found between the dynamics of these boreholes and the riparian zone piezometers, indicating that any potential bias in previous years would be small. The storage change at the catchment was estimated by first calculating the mean January ground water level at each station. The change in level from year to year was interpolated using Thiessen polygons and the mean change was then calculated over the entire catchment.

RESULTS

Evaporation

Annual *E* at the weather station ranged from 380.3–575.3 mm/ year with an average of 505.5 mm/ year. Maximum daily rates of *E* varied from 3.1 mm/ day in 2014 to 5.6 mm/ day in 2015. Excluding months with a large percentage of gap-filled values, *Rn* ($R^2 = 0.91$) and *T* ($R^2 = 0.77$) were the best correlated with monthly *E* measured by the eddy covariance station, with almost no correlation with *P* ($R^2 = 0.08$) and a limited correlation with *SM* ($R^2 = 0.34$) (Figure 6). At the annual timescale, the highest correlation was found for *Rn* ($R^2 = 0.50$, not shown in figure).

Figure 7 shows the daily *E* rates at each eddy covariance station for the year 2020. From January-March *E* rates were low with only small differences between the stations. From April onwards the station located at the winter wheat field started to

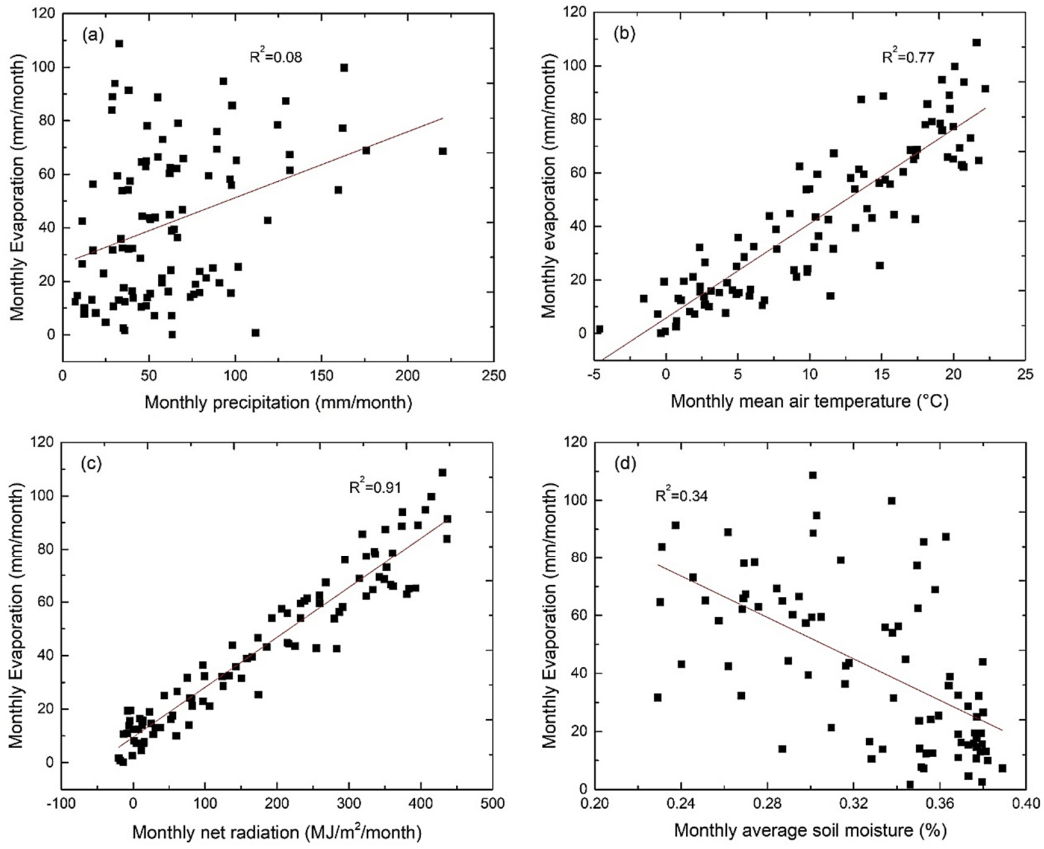

Fig. 6. Scatterplots of (a) monthly sum of precipitation, (b) monthly mean temperature (c) monthly sum of net radiation and (d) monthly mean soil moisture versus the monthly sum of evaporation at the weather station.

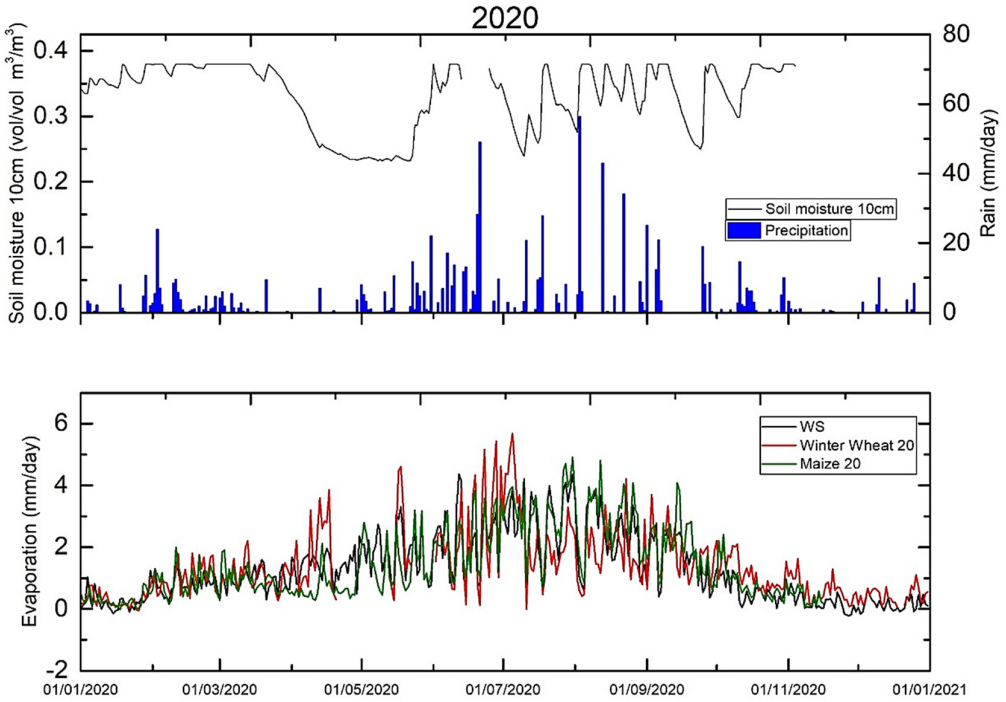

Fig. 7. Daily sums of evaporation at each eddy covariance station (*WS* indicates weather station, the other locations are indicated by the predominant crop type), precipitation (blue bars) and soil moisture (black line) for the year 2020.

measure much higher *E* rates as the crop started to grow, while the grassland weather station also showed an increase in *E*. From April to May the maize field was bare, resulting in low levels of *E* as soil moisture decreased with only a small increase in response to a precipitation event in the middle of April. *E* rates continued to increase at all stations from May until the winter wheat crop was harvested at the beginning of July. From July-September the highest rates were measured at the fully grown maize field until it was harvested at the beginning of October, with much reduced rates measured at the bare winter wheat field. From October onwards a catch crop was grown at the winter wheat field to provide soil cover and fertiliser, resulting in slightly higher *E* values than at the other locations.

Seasonal differences can be seen between the different measurement locations in most years (see Appendix). In 2015 and from 2017–2020 daily differences of up to 2 mm/ day of *E* were measured between locations adjacent to fields containing winter season crops and grassland and bare soil locations, while in 2017, 2018 and 2019 differences of up to 3.1 mm/ day were recorded between fields containing summer crops. In 2014 and 2016 much smaller or no significant differences were seen between the locations, due to the low evaporative demand in 2014 and the high soil moisture during the summer months in 2016. Comparing the mobile stations to the weather station, *Rn* (R^2 = 0.85) and *T* (R^2 = 0.74) were again the environmental variables best correlated with monthly *E*. However, *SM* now showed a much stronger correlation with *E*, R^2 = 0.47 compared to 0.33 at the weather station while *P* also showed increased correlation, it remained much weaker than the other variables (R^2 = 0.15).

Based on this analysis the measurements from the eddy covariance network were then upscaled to the entire catchment as outlined in section Instrumentation and measurements. Figure 8 shows tri-monthly maps of *E* at the catchment for the year 2020. The winter months showed little variation across the catchment, with the largest differences of ~50 mm measured in the July-September period. The upscaled *E* values were then averaged over the entire catchment. Annual values of upscaled *E* (E_{eddy}) over the course of the study ranged from 586.2–420.0 mm/ year with an average of 514.5 mm/ year (Figure 9).

Catchment water balance

Figure 10 shows the yearly values of E_{eddy} and the components of the catchment water balance from 2012–2020, with water balance evaporation, E_{wb}, calculated as the difference between precipitation and discharge. Discharge was relatively constant throughout this period except for a very large increase in 2013 resulting from a high antecedent soil moisture due to snowfall in the previous December continuing into early January coupled with a series of large *P* events in January, May and June (*P* = 220 mm for June). A slight decrease in 2018 and 2019 due to lower *P* amounts was also observed. It can be seen that in years with low *P* amounts there was good agreement between the two estimates, while in years with high *P* amounts there was a clear difference between the E_{wb} and E_{eddy}. To investigate the possible causes for this difference, the groundwater level and storage in the catchment were studied. Figure 11 shows the $E_{wb} - E_{eddy}$ difference between the evaporation estimates against the depth to groundwater level during the summer months. In the years with the smallest $E_{wb} - E_{eddy}$ values the depth to the groundwater level was deepest, while in the years with the largest values of E_{wb} - E_{eddy} the groundwater level was highest, indicating that some of the water was being stored in the groundwater. The storage change was estimated and plotted against $E_{wb} - E_{eddy}$ in Figure 12. The results suggest that in 2015, 2018, 2019 and 2020 the change in storage could account for the difference between the *E* estimates. With the exception of 2020, this corresponded to the years with lower *P* amounts. In the years 2017, 2016 and 2014 however, where higher *P* amounts were measured, the storage change could account for only 41%, 19% and 13% of the discrepancy, while in 2013 the storage change was positive.

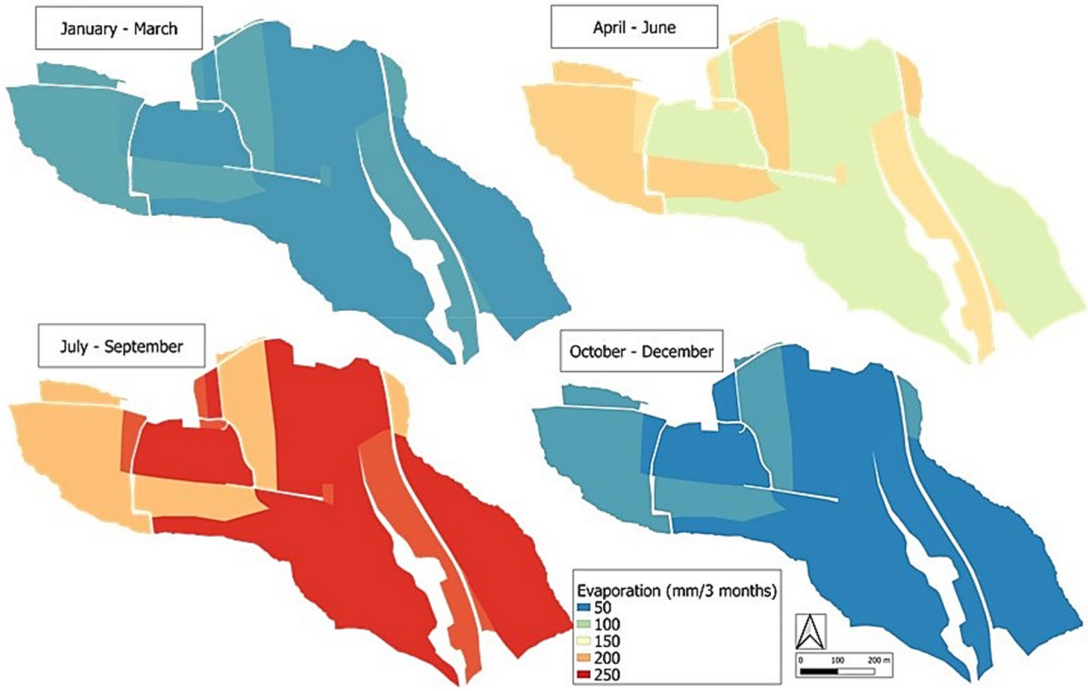

Fig. 8. Tri-monthly maps of evaporation upscaled from each eddy covariance sensor by land use (mm/ 3 months) for the year 2020.

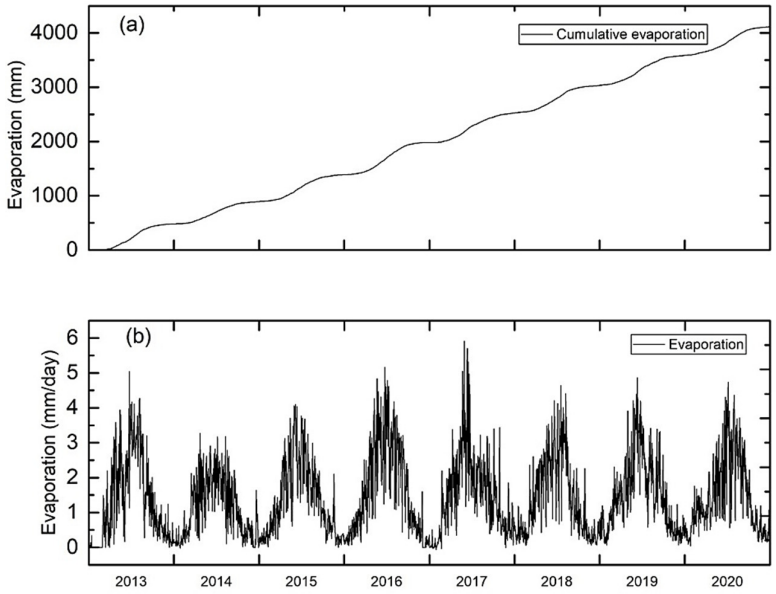

Fig. 9. (a) Cumulative evaporation (mm) and (b) daily values of eddy-covariance-based catchment averaged evaporation (mm/ day) from 2013–2020.

Subcatchment water balances

The average yearly evaporation over the period 2014–2019 was also estimated for each subcatchment using the water balance method (Figure 13). Due to the change in measurement flume in 2019 most of the subcatchments did not give plausible *E* estimates in 2020 and were not included in the calculation. The largest estimates were from the subcatchments corresponding to agricultural (Sys4 Max, Frau2) and mixed forest-agriculture (Sys3 Max) land use.

The yearly values of *E* estimated using the subcatchments/ water balance (E_{sub}), and by the eddy covariance measurements/ land use (E_{lu}) are compared in Figure 14. With the exception of Sys4 Max which gave consistently higher estimates of *E*, the two methods gave similar results. The spatial distribution of E_{wb} was homogenous in the eastern side of the catchment along the riparian zone, with only small differences between the subcatchments (A2, Sys2, Sys3 Max) in most years. In 2017 *E* ranged between 509 and 521 mm and between 505 and 536 mm in 2018, while in 2015 the A2 catchment dried out over

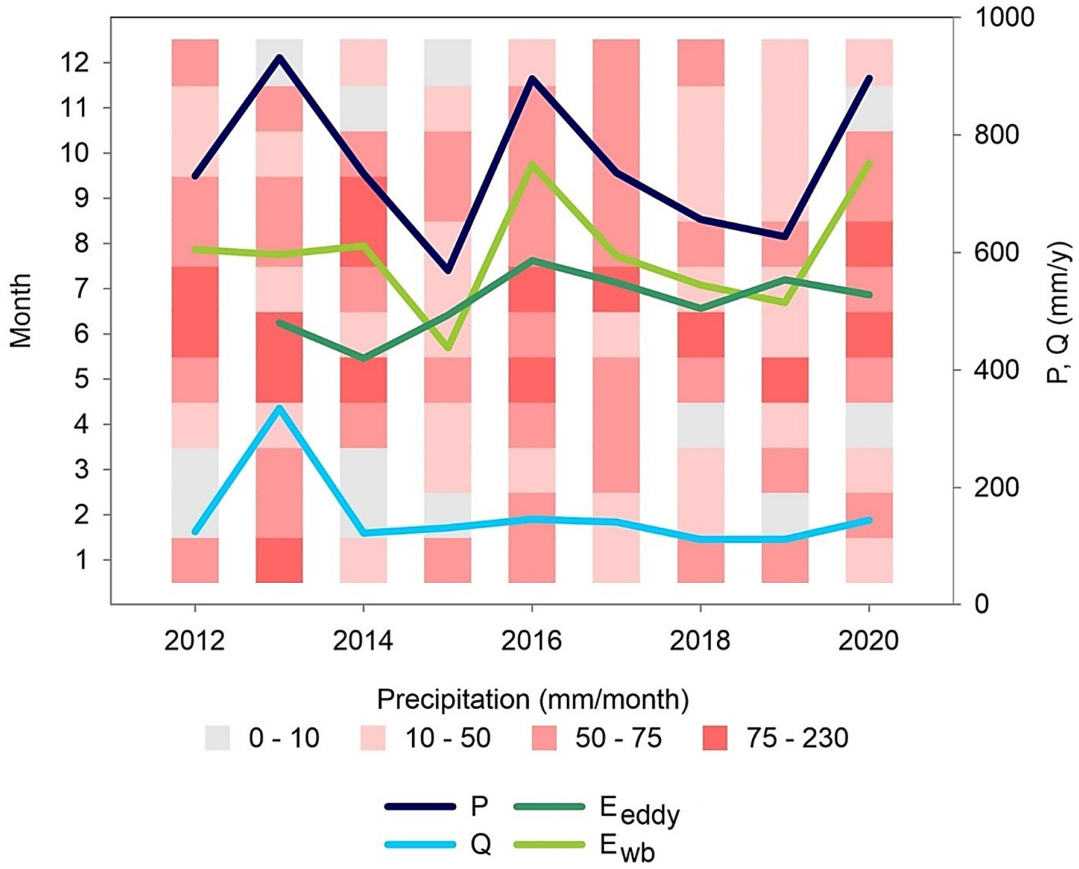

Fig. 10. The components of the catchment water balance displayed over the monthly distribution of precipitation for the years 2012–2020. The red vertical bars show the monthly distribution of *P* for each year. On the right axis the yearly sums of: eddy covariance evaporation E_{eddy} (dark green line), water balance evaporation E_{wb} (light green line), outlet discharge *Q* (light blue line) and *P* (dark blue line) for the entire catchment area are displayed for each year.

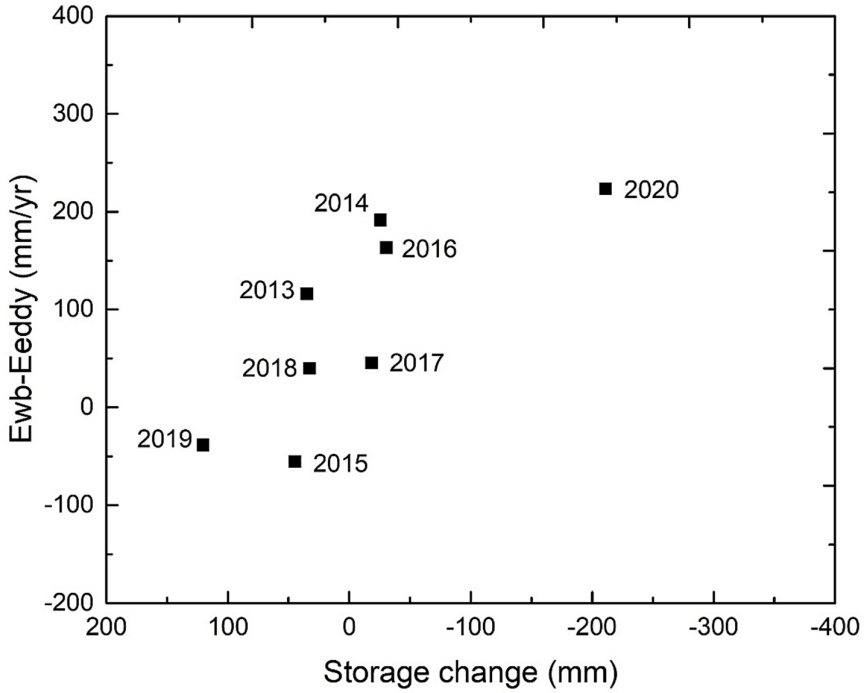

Fig. 11. The yearly gap between the water balance based and the eddy-covariance-based evaporation estimates plotted against the summer/early autumn average (June–September) depth to groundwater level measured at a deeper riparian piezometer (H01).

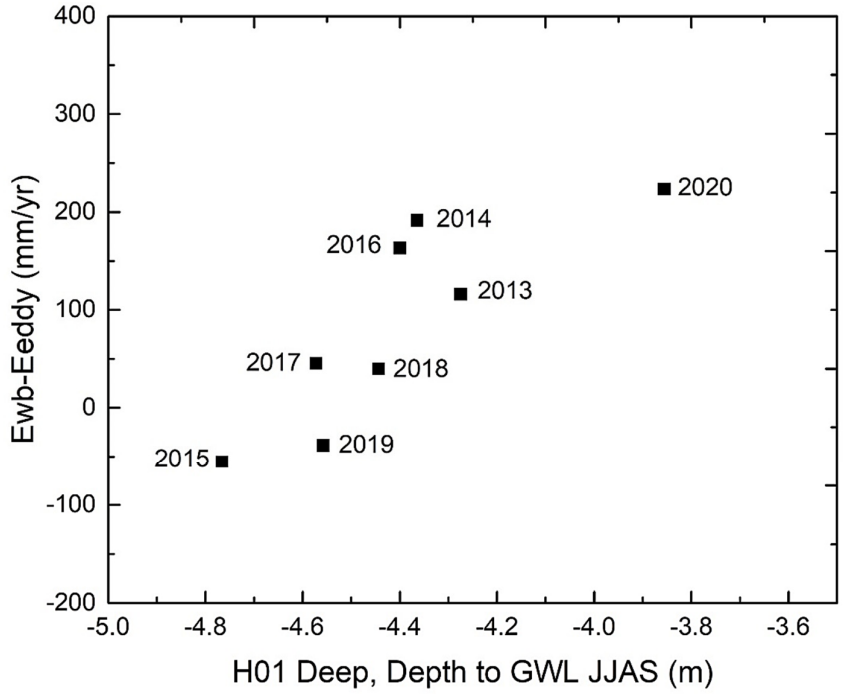

Fig. 12. The yearly gap between the water balance based and the eddy-covariance-based evaporation estimates plotted against the yearly catchment averaged storage change.

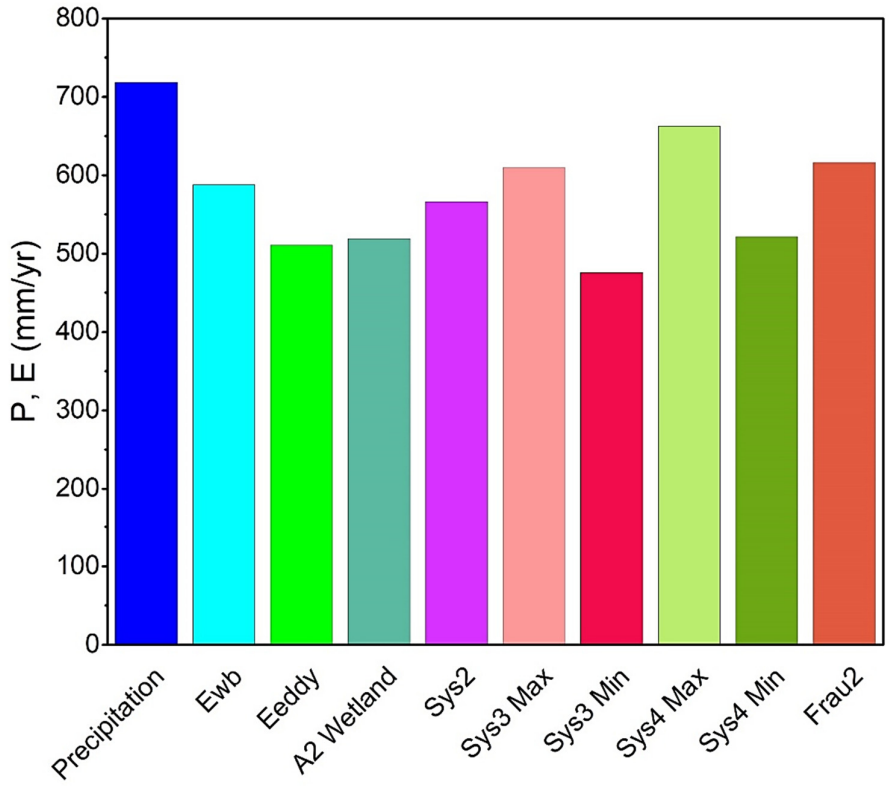

Fig. 13. Average yearly precipitation and evaporation E (2014–2019), calculated from the catchment water balance for the entire catchment (E_{wb}), for each subcatchment, and the catchment averaged eddy covariance-based-estimate (E_{eddy}).

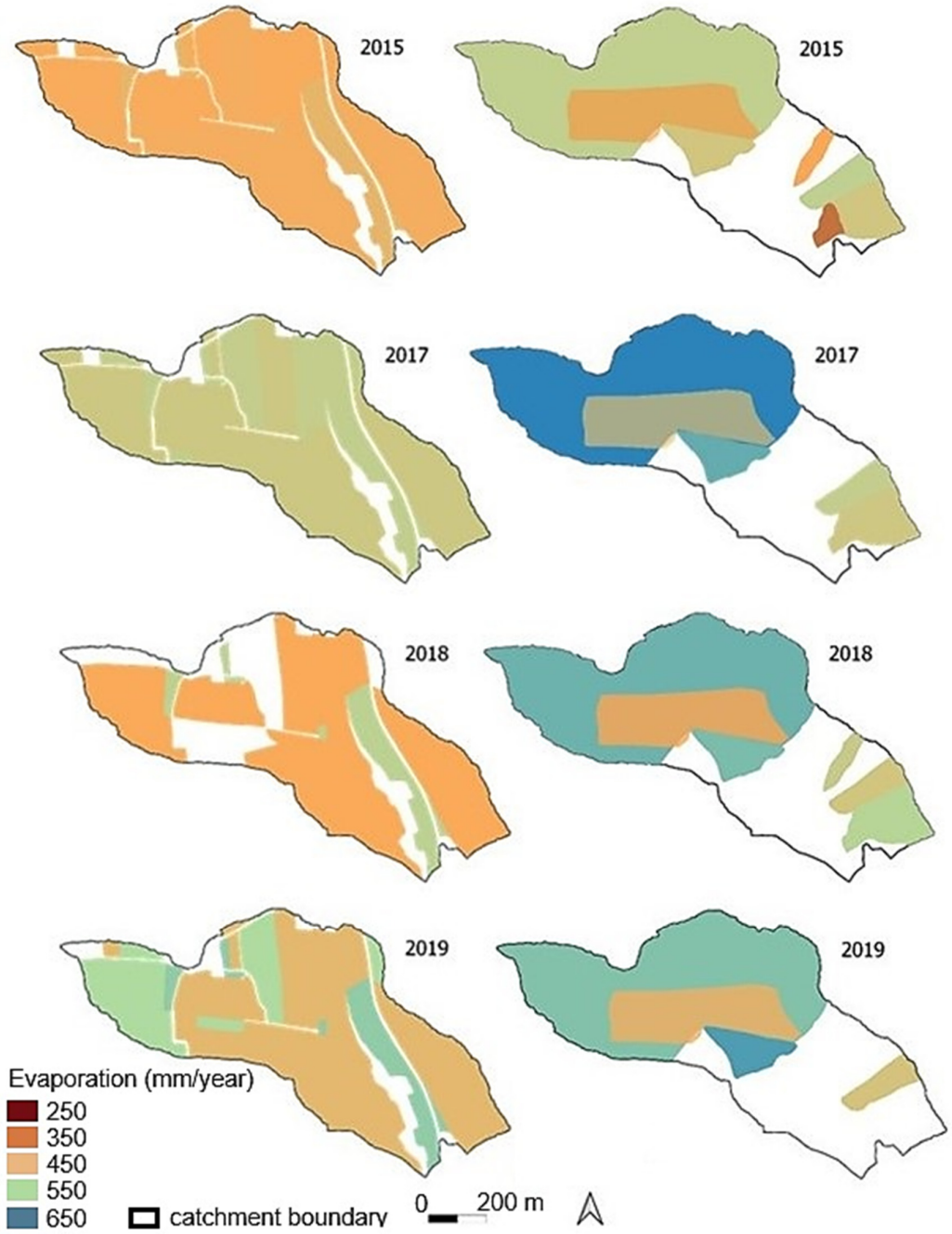

Fig. 14. Yearly maps of (left) evaporation upscaled from each eddy covariance sensor by land use and (right) subcatchment water balance method-based evaporation for each tributary, for years where the catchment water balance residual < 100 mm. White space indicates no data available.

the course of the summer due to the low amounts of *P* resulting in a lower *E* estimate of 450 mm compared to 526 and 506 mm for the Sys2 and Sys3 Max catchments.

Each subcatchment was compared with the most representative eddy covariance land use estimate in Figure 15. A2 showed a slight correlation with measured *E* from the grassland area ($R^2 = 0.27$). In 2016 and 2017 only very small amounts of runoff were measured. Sys 1 showed no correlation with measured *E*. There was also a gradual decrease in the ratio of precipitation to runoff from 2013–2018. Sys3 Min showed a much higher correlation with measured *E* than Sys2 and Sys3 Max ($R^2 = 0.35$ versus $R^2 = 0.19$ and $R^2 = 0.03$). Sys3 Min also estimated similar levels of *E* on a yearly basis compared to the catchment average *E*, with Sys2 and only providing a similar estimate for 2015, 2017 and 2018, and Sys3 Max in 2015. There was a large uncertainty in the catchment area for Sys4. The maximum catchment area was more strongly correlated with *E* measured over the crop fields compared to the minimum area ($R^2 = 0.32$ versus $R^2 = 0.18$), however, Sys4 Min showed much better agreement in yearly *E*. Frau 2 is a tile drainage system within a crop field. As it is mainly activated during rainfall events with only a small base flow, it results in low amounts of measured runoff and hence high *E* estimates.

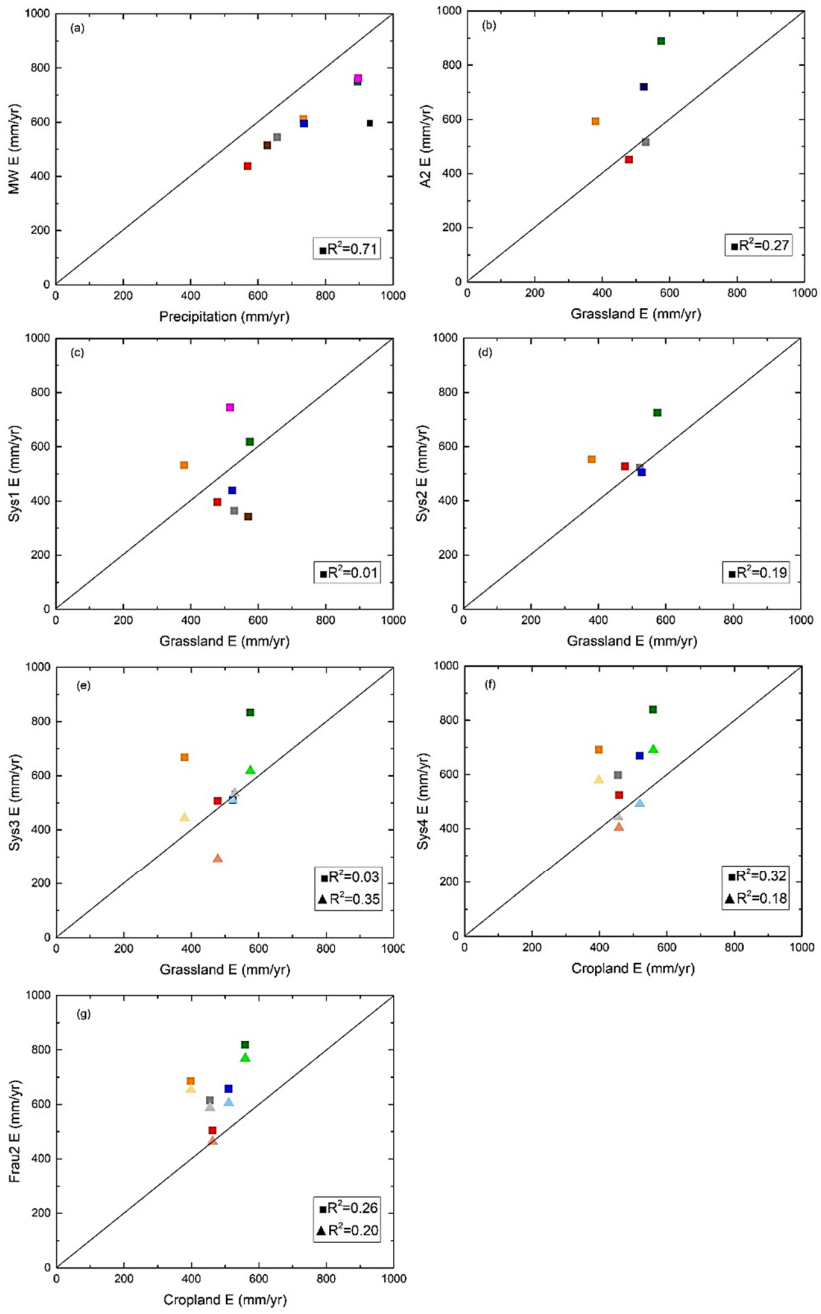

Fig. 15. Scatterplots of subcatchment water balance ET versus (a) precipitation and (b-g) evaporation *E* measured at the most representative eddy covariance station. Squares represent maximum catchment area estimates and triangles minimum catchment area estimates, with individual years coloured according to: 2013 (black, MW only), 2014 (yellow), 2015 (red), 2016 (green), blue (2017), grey (2018), 2019 (brown, MW only), 2020 (purple, MW and Sys1 only).

DISCUSSION

At the daily and monthly timescales, spatial patterns could be seen between the eddy covariance stations. These were due to changes in land cover resulting from the agricultural land use cycle and resulting variations in leaf and root area density. The largest differences, up to 3 mm/ day, were seen between bare fields and fully grown crops during dry summer months (July–September). This is consistent with other studies conducted over shorter time periods, with Hssaine et al. (2021) reporting differences of greater than 4 mm/ day between harvested and irrigated fields in a semi-arid climate. These large differences at small scales are of particular importance for remote sensing methods of estimating *E,* where the measurement pixel may incorporate different land uses and irrigation patterns, as well as having an infrequent sampling rate (Anderson et al., 2012). From late autumn to early spring, *E* rates tended to be low due to the reduced temperature and incoming solar radiation. Only small spatial differences were measured between the stations, as the low amounts of evaporation resulted in a homogeneous soil

moisture distribution across the catchment. Zhang et al. (2010) reported similar differences between seasons in reference evapotranspiration when modelled at the basin scale, with low variation from December-February and highest from May-August. At the annual scale, reduced patterns of *E* were found between fields, as the higher *E* rates during the vegetated periods tended to be balanced out by the reduced rates during the non-vegetated periods.

At the subcatchments located primarily within the riparian zone (Sys2, Sys3 and A2), annual differences in *E* connected to the presence of permanent vegetation with roots able to access the groundwater resulted in higher *E* estimates than at the grassland-wetland subcatchment (A2). The latter tended to dry out in drier years, as in 2015. In the following years the larger precipitations amount of 2016, 2017 and 2018 gradually recharged the subsurface aquifers, resulting in runoff occurring here again in 2018. Sys1 showed no correlation with measured *E*. There was also a gradual decrease in the ratio of *P* to runoff from 2013 to 2018. Following this and the findings of Exner-Kittridge et al. (2016) Sys1 could be characterised as a deep aquifer system. There is a large groundwater component to the runoff which is independent of the dryness of the unsaturated zone, resulting in Sys1 being unaffected by the meteorological drivers of evaporation. This is in contrast to the nearby A2 where the contributing flow paths run closer to the surface. The large level of disagreement between the estimates for the two catchment areas of Sys3, with Sys3 Min providing a more similar *E* estimate to eddy covariance *E* in certain years and Sys3 Max in others, would suggest that the catchment area is changing in certain years. Széles et al. (2018) found that the vegetation influence on streamflow during rainless periods was higher at Sys3 compared to Sys2. This was explained by the difference in soil types and dominant trees species. At Sys3 the soil was well watered, and the roots of the trees were well connected to the groundwater levels. Sys4 runs through the entire year with a comparatively high base flow component, while the catchment area is covered predominantly by crop fields. Sys4 Max gave considerably higher estimates of *E* than Sys4 Min. As the crop fields have a larger influence on the subcatchment water balance than at the other subcatchments, there was good agreement between the catchment average and water balance estimates for years with relatively low *P* and high *E* (2015, 2017, 2018 and 2019). Combined with the large groundwater component, this resulted in this tributary behaving similarly to the main catchment. Due to the low but permanent runoff during the entire year, Frau2 was partly influenced by evapotranspiration from the crops, which are the dominant land use type for this subcatchment, showing a lower correlation to measured *E* compared to Sys4. In both the agricultural and the riparian areas detailed land use and vegetation information is needed when small catchments are to be studied or modelled, with evaporation patterns forming according to the crop cycle in the agricultural areas and the vegetation in the riparian zone.

Interannual differences of –13–27% were measured at the catchment level between the upscaled eddy covariance and water balance methods, which fell outside the –10 to 17% range reported by Scott (2010) over a 5-year period and –7–11% estimated by Denager et al. (2020) over a 3-year period. In these catchments however no significant groundwater flow or storage was reported. Tie et al. (2018) found differences of up to 20% at a mountainous catchment which were attributed to groundwater flow. When storage was estimated during years with above average *P*, year to year variability of the catchment evaporation methods was consistent ($R^2 = 0.80$ when accounted for versus $R^2 = 0.37$ when not). The results show the importance of, and provide a method for testing the water balance method for non-closure and leakage, by measuring and upscaling the evaporation using the eddy covariance method and vegetation. Further work is required to investigate the nature of the leakage, and when and where in the catchment it occurs.

In this study *E* was upscaled according to land use and crop type, assuming that the *E* measured at an eddy covariance station in a certain crop type was valid for other fields within the catchment with the same crop. Net radiation and temperature were found to be the main drivers of monthly *E* measured by the weather station and mobile eddy covariance stations, with almost no correlation with *P*. The biggest difference between the stations was found to be due to soil moisture, with the mobile stations showing a larger correlation than the weather station. The land use at the weather station is meadow which is subjected to minimal management. This results in a lower dependency on soil moisture for evaporation compared to the mobile stations where the crops are regularly harvested, resulting in bare surfaces where the evaporation is limited by the soil moisture near the surface. At the field scale net radiation was also found to be the main environmental driver of crop transpiration by Zhou et al. (2019). At the annual timescale, *Rn* was also the main driver for the eddy covariance-based estimate method ($R^2 = 0.50$), however *P* was the main driver of the water balance-based E estimate ($R^2 = 0.81$). At the field scale Mo et al. (2004) and Hatfield and Prueger (2011) observed that spatial variation in *Rn* and *P* due to cumulus clouds and the resulting variation in energy and soil moisture led to patterns in *E* between fields of the same crop type across a small watershed. Due to the much smaller size of our catchment (66 vs 5,400 ha) and with cumulus clouds having a typical linear dimension of 3–10 km (Weisman and Klemp, 1986) it is unlikely that such variation could affect the upscaling. While a soil moisture network was installed within the catchment the number of stations located within the agricultural fields was limited, and in addition these sensors had to be removed and reinstalled before and after land management practices.

The results emphasize the importance of detailed and updated land use information; land use data tends to be static or limited in temporal resolution at larger scales, which in patchwork agricultural landscapes can result in incorrect evaporation model estimates. Particularly in the case where the spatial land use patterns combine with temporal patterns of the main meteorological drivers, suggested from the results of this study as: net radiation, temperature and precipitation. When planning short-term to seasonal length experiments however, the influence of patterns generated by the land use cycle, particularly non-permanent vegetation such as crops, needs to be taken into account when choosing an installation site for the devices. For long-term observations in catchments consisting of different types of permanent vegetation and/ or different runoff generation mechanism, singular measurements of evaporation with a limited footprint, such as eddy covariance, should be used to support distributed measurements, such as subcatchment gauging, by providing a control for evaporation for subcatchments where the surface vegetation tends to become disconnected from the groundwater. Additionally, evaporation estimated using water balance measurements should be controlled with alternative evaporation measurements or model estimates in years with high amounts of precipitation. In areas with pronounced topographical or soil texture differences, differences in the soil moisture content may result in short term evaporation patterns following precipitation events when leaf area is low, either during the early growing stages of densely planted crops or for crops with a wide row spacing.

CONCLUSIONS

In this study the spatial patterns of evaporation and their drivers in a small agricultural catchment were investigated at monthly to yearly timescales. Spatial differences can be seen between subcatchments at different timescales and are consistent between the methods. Seasonal patterns can be seen between the eddy covariance stations due to changes in land cover resulting from the agricultural land use cycle due to the variations in leaf and root area density during the growing season.

Year to year variability in monthly *E* measured by the eddy covariance stations was driven primarily by net radiation and temperature. Precipitation was the main driver of annual water balance-based *E* estimate, versus net radiation for the annual eddy covariance-based estimate method. Year to year variability of the catchment evaporation methods is consistent, only when storage and leakage are estimated during years with above average precipitation. In these years the catchment water balance method overestimates *E* and in catchments with similar hydrological conditions, an additional independent estimate of *E* should be recommended in similar years.

The results indicate that at daily and monthly timescales information on land cover and soil moisture is important in order to correctly estimate *E* in catchments with agricultural vegetation, particularly when the basic data are sampled infrequently, such as during satellite overpasses, as changes in land use result in large variations in *E*.

Acknowledgements. The authors would like to acknowledge financial support provided by the Austrian Science Funds (FWF) as part of the Vienna Doctoral Program on Water Resource Systems (DK W1219-N28) and as part of the project IRISE (Project number I 6254-N), by the Slovenian Research and Innovation Agency (ARIS) (Project number J2-4489), and by the HOAL2.0 project.

RERENCES

Allen, R.G., Pereira, L.S., Raes, D., Smith, M., 1998. Crop Evapotranspiration - Guidelines for Computing Crop Water Requirements. FAO Irrigation and drainage paper 56. Food and Agriculture Organization of the United Nations, Rome, Italy.

Anderson, M.C., Kustas, W.P., Alfieri, J.G., Gao, F., Hain, C., Prueger, J.H., Evett, S., Colaizzi, P., Howell, T., Chavez, J.L., 2012. Mapping daily evapotranspiration at Landsat spatial scales during the BEAREX'08 field campaign. Advances in Water Resources, 50, 162–177.

Armstrong, R.N., Pomeroy, J.W., Martz, L.W., 2019. Spatial variability of mean daily estimates of actual evaporation from remotely sensed imagery and surface reference data. Hydrology and Earth System Sciences, 23, 4891–4907.

Bastiaanssen, W.G.M., Noordman, E.J.M., Pelgrum, H., Davids, G., Thoreson, B.P., Allen, R.G., 2005. SEBAL model with remotely sensed data to improve water-resources management under actual field conditions. Journal of Irrigation and Drainage Engineering, 131, 1, 85–93.

Blöschl, G., Blaschke, A.P., Broer, M., Bucher, C., Carr, G., Chen, X., Eder, A., Exner-Kittridge, M., Farnleitner, A., Flores-Orozco, A., Haas, P., Hogan, P., Kazemi Amiri, A., Oismüller, M., Parajka, J., Silasari, R., Stadler, P., Strauss, P., Vreugdenhil, M., Wagner, W., Zessner, M., 2016. The Hydrological Open Air Laboratory (HOAL) in Petzenkirchen: a hypothesis-driven observatory. Hydrology and Earth System Sciences, 20, 227–255.

Bouwer, L.M., Biggs, T.W., Aerts, J.C.J.H., 2008. Estimates of spatial variation in evaporation using satellite-derived surface temperature and a water balance model. Hydrological Processes, 22, 5, 670–682.

Denager, T., Looms, M.C., Sonnenborg, T.O., Jensen, K.H., 2020. Comparison of evapotranspiration estimates using the water balance and the eddy covariance methods. Vadose Zone Journal, 19, 1, e20032.

Eshonkulov, R., Poyda, A., Ingwersen, J., Wizemann, H.-D., Weber, T.K.D., Kremer, P., Högy, P., Pulatov, A., Streck, T., 2019. Evaluating multi-year, multi-site data on the energy balance closure of eddy-covariance flux measurements at cropland sites in southwestern Germany. Biogeosciences, 16, 2, 521–540.

Eswar, R., Sekhar, M., Bhattacharya, B.K., 2017. Comparison of three remote-sensing-based models for the estimation of latent heat flux over India. Hydrological Sciences Journal, 62, 16, 2705–2719.

Exner-Kittridge, M., Strauss, P., Blöschl, G., Eder, A., Saracevic, E., Zessner, M., 2016. The seasonal dynamics of the stream sources and input flow paths of water and nitrogen of an Austrian headwater agricultural catchment. Science of the Total Environment, 542, Part A, 935–945.

Fischer, M., Trnka, M., Hlavinka, P., Orság, M., Kučera, J., Žalud, Z., 2011. Identifying the Fao-56 crop coefficient for high density poplar plantation: the role of interception in estimation of evapotranspiration. In: Šiška, B., Hauptvogl, M., Eliašová, M. (eds.). Bioclimate: Source and Limit of Social Development International Scientific Conference. Topoľčianky, Slovakia.

Foken, T., 2008. The energy balance closure problem: An overview. Ecological Applications, 18, 6, 1351–1367.

Hatfield, J.L., Prueger, J.H., 2011. Spatial and Temporal Variation in Evapotranspiration, Evapotranspiration - From Measurements to Agricultural and Environmental Applications. IntechOpen, 10.5772/17852.

Hssaine, B., Chehbouni, A., Er-Raki, S., Khabba, S., Ezzahar, J., Ouaadi, N., Ojha, N., Rivalland, V., Merlin, O., 2021. On the utility of high-resolution soil moisture data for better constraining thermal-based energy balance over three semi-arid agricultural areas. Remote Sensing, 13, 4, 727.

Imukova, K., Ingwersen, J., Hevart, M., Streck, T., 2016. Energy balance closure on a winter wheat stand: comparing the eddy covariance technique with the soil water balance method. Biogeosciences, 13, 1, 63–75.

Jiang, Z.-Y., Yang, Z.-G., Zhang, S.-Y., Liao, C.-M., Hu, Z.-M., Cao, R.-C., Wu, H.-W., 2020. Revealing the spatio-temporal variability of evapotranspiration and its components based on an improved Shuttleworth-Wallace model in the Yellow River Basin. Journal of Environmental Management, 262, 110310.

Kustas, W.P., Hatfield, J.L., Prueger, J.H., 2005. The soil moisture-atmosphere coupling experiment (SMACEX): background, hydrometeorological conditions, and preliminary findings. Journal of Hydrometeorology, 6, 6, 791–804.

Leuning, R., van Gorsel, E., Massman, W.J., Isaac, P.R., 2012. Reflections on the surface energy imbalance problem. Agricultural and Forest Meteorology, 156, 65–74.

Liang, L., Li, L., Liu, Q., 2011. Spatio-temporal variations of reference crop evapotranspiration and pan evaporation in the West Songnen Plain of China. Hydrological Sciences Journal, 56, 7, 1300–1313.

Mauder, M., Liebethal, C., Göckede M., Leps, J.-P., Beyrich, F., Foken, T., 2006. Processing and quality control of flux data

during the LITFASS-2003. Boundary-Layer Meteorology, 121, 67–88.

Mauder, M., Foken, T., 2015. Eddy-Covariance Software TK3. In Documentation and Instruction Manual of the Eddy-Covariance Software Package TK3 (update). University of Bayreuth, 67 p.

Mo, X., Liu, S., Lin, Z., Zhao, W., 2004. Simulating temporal and spatial variation of evapotranspiration over the Lushi basin. Journal of Hydrology, 285, 1–4, 125–142.

Moore, C.J., 1986. Frequency response corrections for eddy correlation systems. Boundary-Layer Meteorology, 37, 17–35.

Prueger, J.H., Hatfield, J.L., Parkin, T.B., Kustas, W.P., Hipps, L.E., Neale, C.M.U., MacPherson, J.I., Eichinger, W.E., Cooper, D.I., 2005. Tower and aircraft eddy covariance measurements of water vapor, energy, and carbon dioxide fluxes during SMACEX. Journal of Hydrometeorology, 6, 6, 954–960.

Ruhoff, A.L., Paz, A.R., Aragao, L.E.O.C., Mu, Q., Malhi, Y., Collischonn, W., Rocha, H.R., Running, S.W., 2013. Assessment of the MODIS global evapotranspiration algorithm using eddy covariance measurements and hydrological modelling in the Rio Grande basin. Hydrological Sciences Journal, 58, 8, 1658–1676.

Schotanus, P., Nieuwstadt, F.T.M., De Bruin, H.A.R., 1983. Temperature measurement with a sonic anemometer and its application to heat and moisture fluxes. Boundary-Layer Meteorology, 26, 81–93.

Scott, R.L., 2010. Using watershed water balance to evaluate the accuracy of eddy covariance evaporation measurements for three semiarid ecosystems. Agricultural and Forest Meteorology, 150, 2, 219–225.

Shimizu, T., Kumagai, T., Kobayashi, M., Tamai, K., Iida, S., Kabeya, N., Ikawa, R., Tateishi, M., Miyazawa, Y., Shimizu, A., 2015. Estimation of annual forest evapotranspiration from a coniferous plantation watershed in Japan (2): Comparison of eddy covariance, water budget and sap-flow plus interception loss. Journal of Hydrology, 522, 250–264.

Széles, B., Broer, M., Parajka, J., Hogan, P., Eder, A., Strauss, P., Blöschl, G., 2018. Separation of scales in transpiration effects on low flows: A spatial analysis in the hydrological open air laboratory. Water Resources Research, 54, 9, 6168–6188.

Tie, Q., Hu, H., Tian, F., Holbrook, N.M., 2018. Comparing different methods for determining forest evapotranspiration and its components at multiple temporal scales. Science of the Total Environment, 633, 12–29.

Valayamkunnath, P., Sridhar, V., Zhao, W., Allen, R.G., 2018. Intercomparison of surface energy fluxes, soil moisture, and evapotranspiration from eddy covariance, large-aperture scintillometer, and modeling across three ecosystems in a semiarid climate. Agricultural and Forest Meteorology, 248, 22–47.

Webb, E.K., Pearman, G.I., Leuning, R., 1980. Correction of flux measurements for density effects due to heat and water vapour transfer. Quarterly Journal of the Royal Meteorological Society, 106, 447, 85–100.

Weisman, M.L., Klemp, J.B., 1986. Characteristics of isolated convective storms. In: Ray, P.S. (ed.): Mesoscale Meteorology and Forecasting, Ch. 15. American Meteorological Society, Boston, MA, pp. 331–358.

Wilson, K.B., Hanson, P.J., Mulholland, P.J., Baldocchi, D.D., Wullschleger, S.D., 2001. A comparison of methods for determining forest evapotranspiration and its components: sap-flow, soil water budget, eddy covariance and catchment water balance. Agricultural and Forest Meteorology, 106, 2, 153–168.

Wilson, K., Goldstein, A., Falge, E., Aubinet, M., Baldocchi, D., Berbigier, P., Bernhofer, C., Ceulemans, R., Dolman, H., Field, C., Grelle, A., Ibrom, A., Law, B.E., Kowalski, A., Meyers, T., Moncrieff, J., Monson, R., Oechel, W., Tenhunen, J., Valentini, R., Verma, S., 2002. Energy balance closure at FLUXNET sites. Agricultural and Forest Meteorology, 113, 1–4, 223–243.

Xu, C., Gong, L., Jiang, T., Chen, D., Singh, V.P., 2006. Analysis of spatial distribution and temporal trend of reference evapotranspiration and pan evaporation in Changjiang (Yangtze River) catchment. Journal of Hydrology, 327, 1–2, 81–93.

Zhang, X., Kang, S., Zhang, L., Liu, J., 2010. Spatial variation of climatology monthly crop reference evapotranspiration and sensitivity coefficients in Shiyang river basin of northwest China. Agricultural Water Management, 97, 10, 1506–1516.

Zhang, Z., Tian, F., Hu, H., Yang, P., 2014. A comparison of methods for determining field evapotranspiration: photosynthesis system, sap flow, and eddy covariance. Hydrology and Earth System Sciences, 18, 3, 1053–1072.

Zhou, L., Wang, Y., Jia, Q., Li, R., Zhou, M., Zhou, G., 2019. Evapotranspiration over a rainfed maize field in northeast China: How are relationships between the environment and terrestrial evapotranspiration mediated by leaf area? Agricultural Water Management, 221, 538–546.

Received 28 June 2024
Accepted 23 October 2024

APPENDIX

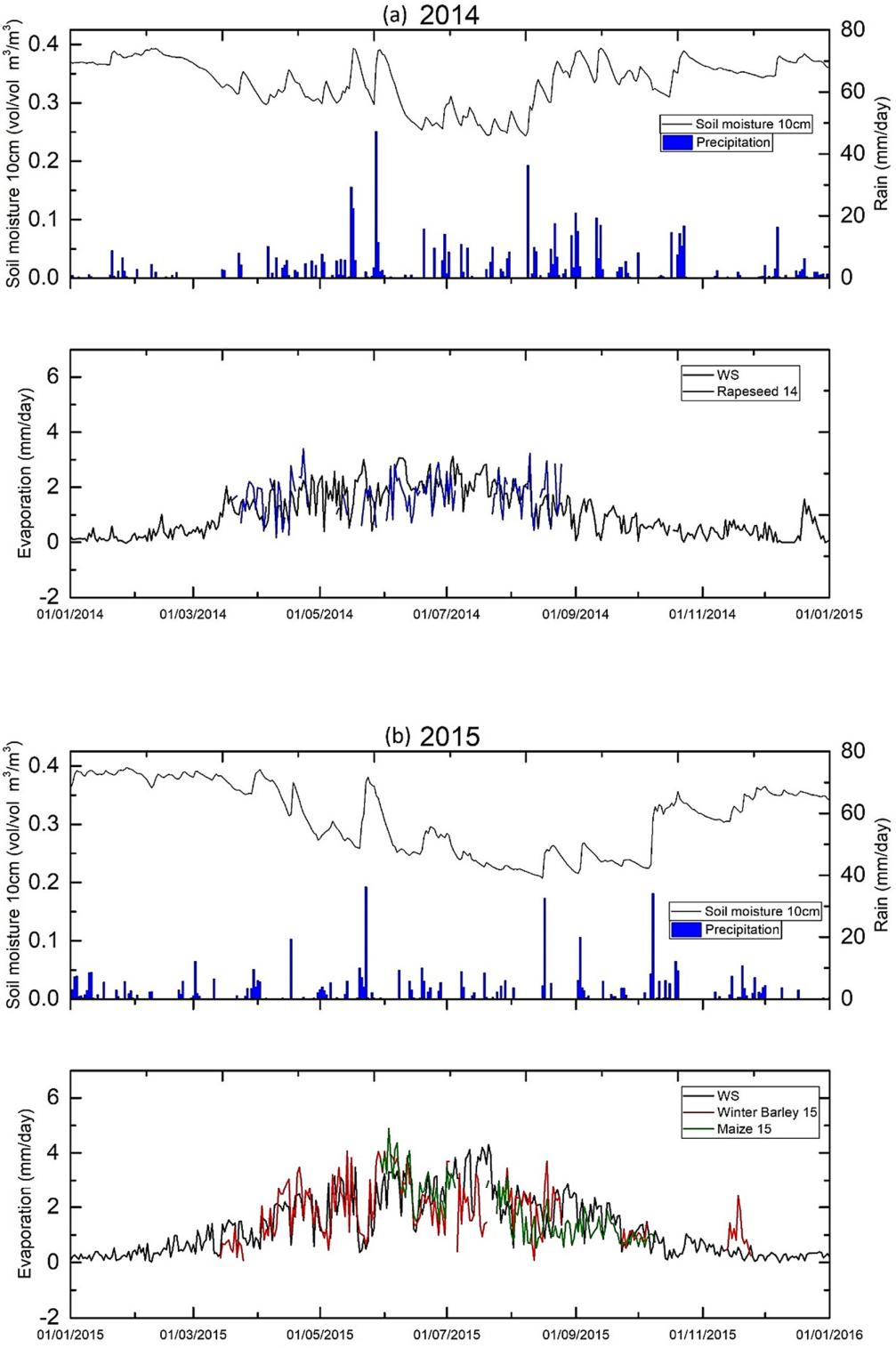
(a) 2014
Soil moisture 10cm (vol/vol m³/m³)
Rain (mm/day)
Soil moisture 10cm
Precipitation
Evaporation (mm/day)
WS
Rapeseed 14
01/01/2014
01/03/2014
01/05/2014
01/07/2014
01/09/2014
01/11/2014
01/01/2015
(b) 2015
Soil moisture 10cm (vol/vol m³/m³)
Rain (mm/day)
Soil moisture 10cm
Precipitation
Evaporation (mm/day)
WS
Winter Barley 15
Maize 15
01/01/2015
01/03/2015
01/05/2015
01/07/2015
01/09/2015
01/11/2015
01/01/2016

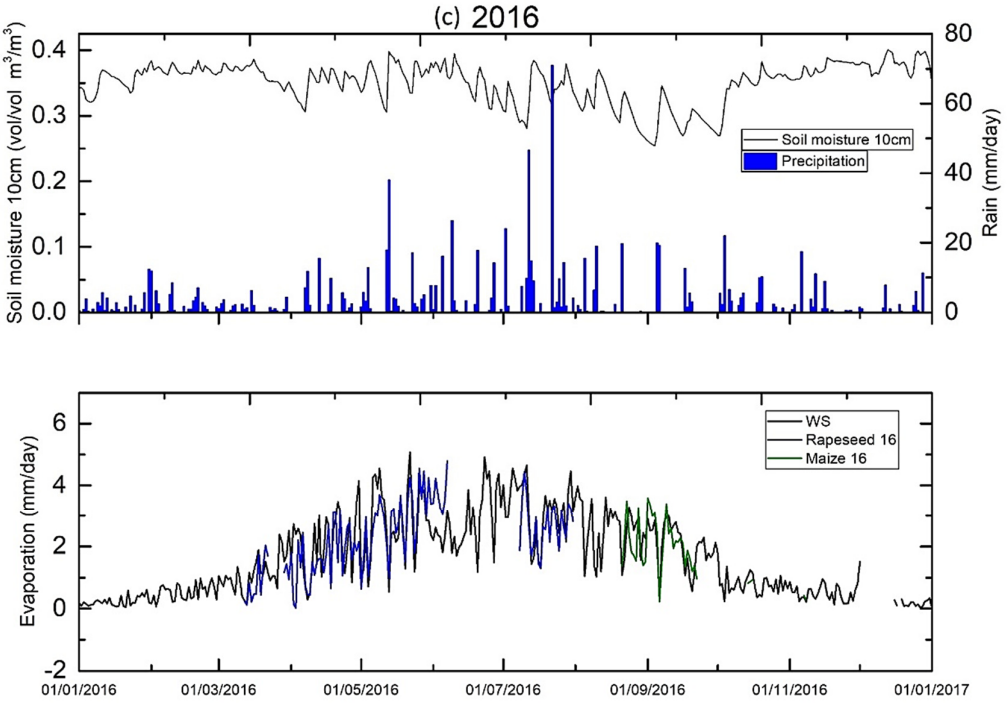
(c) 2016
Soil moisture 10cm (vol/vol m³/m³)
Rain (mm/day)
Soil moisture 10cm
Precipitation
Evaporation (mm/day)
WS
Rapeseed 16
Maize 16
01/01/2016
01/03/2016
01/05/2016
01/07/2016
01/09/2016
01/11/2016
01/01/2017

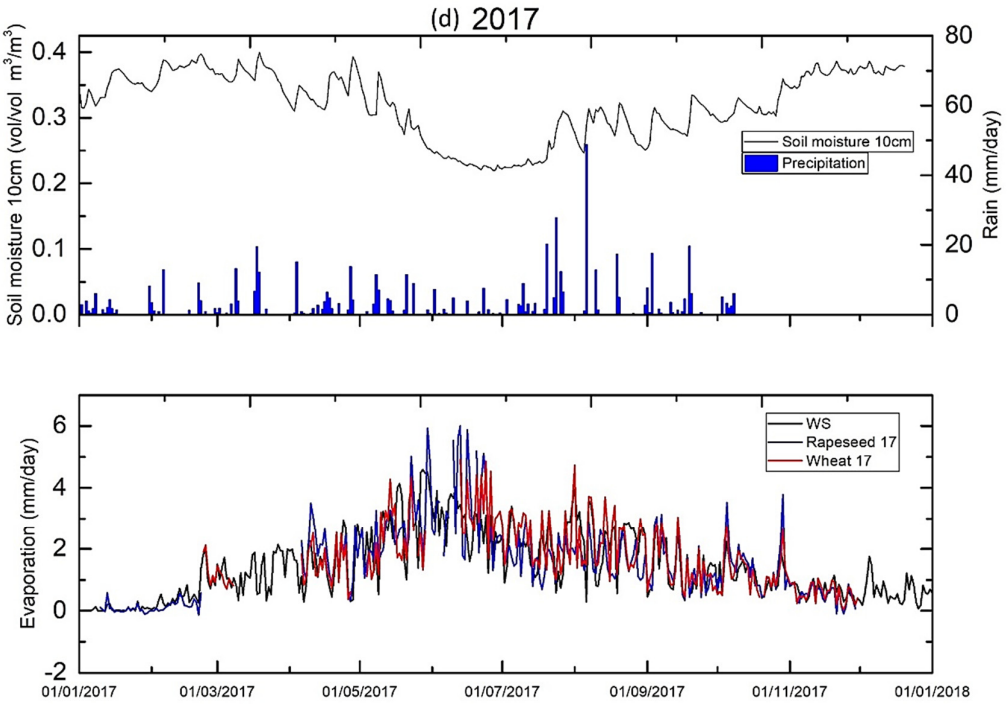
(d) 2017
Soil moisture 10cm (vol/vol m³/m³)
Rain (mm/day)
Soil moisture 10cm
Precipitation
Evaporation (mm/day)
WS
Rapeseed 17
Wheat 17
01/01/2017
01/03/2017
01/05/2017
01/07/2017
01/09/2017
01/11/2017
01/01/2018

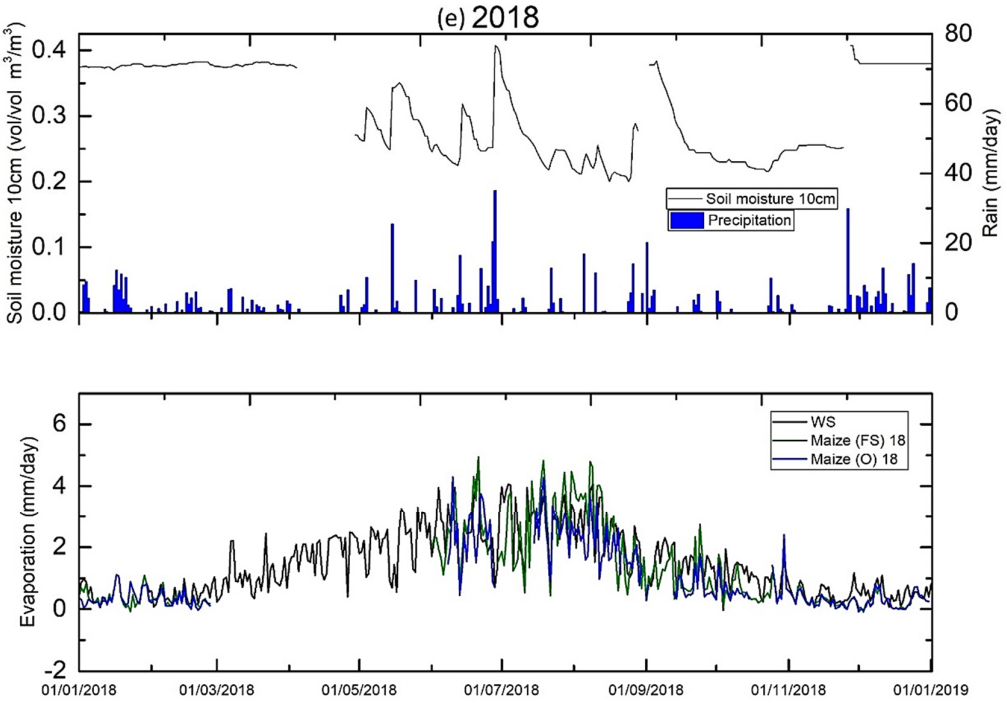
(e) 2018
Soil moisture 10cm (vol/vol m³/m³)
Rain (mm/day)
Soil moisture 10cm
Precipitation
Evaporation (mm/day)
WS
Maize (FS) 18
Maize (O) 18
01/01/2018
01/03/2018
01/05/2018
01/07/2018
01/09/2018
01/11/2018
01/01/2019

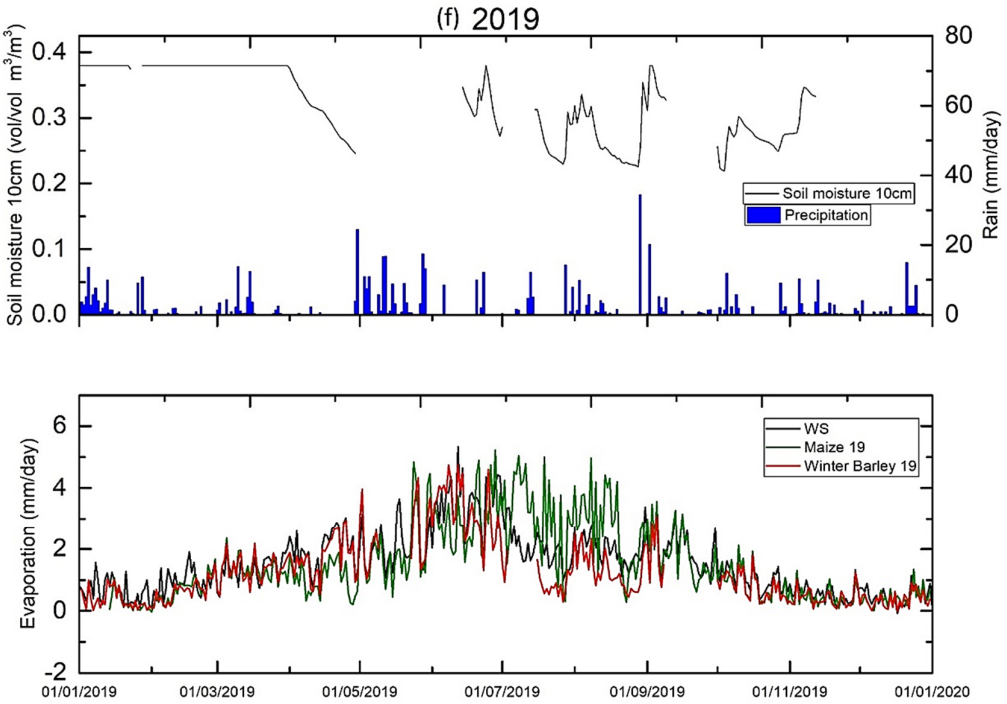
(f) 2019
Soil moisture 10cm (vol/vol m³/m³)
Rain (mm/day)
Soil moisture 10cm
Precipitation
Evaporation (mm/day)
WS
Maize 19
Winter Barley 19
01/01/2019
01/03/2019
01/05/2019
01/07/2019
01/09/2019
01/11/2019
01/01/2020

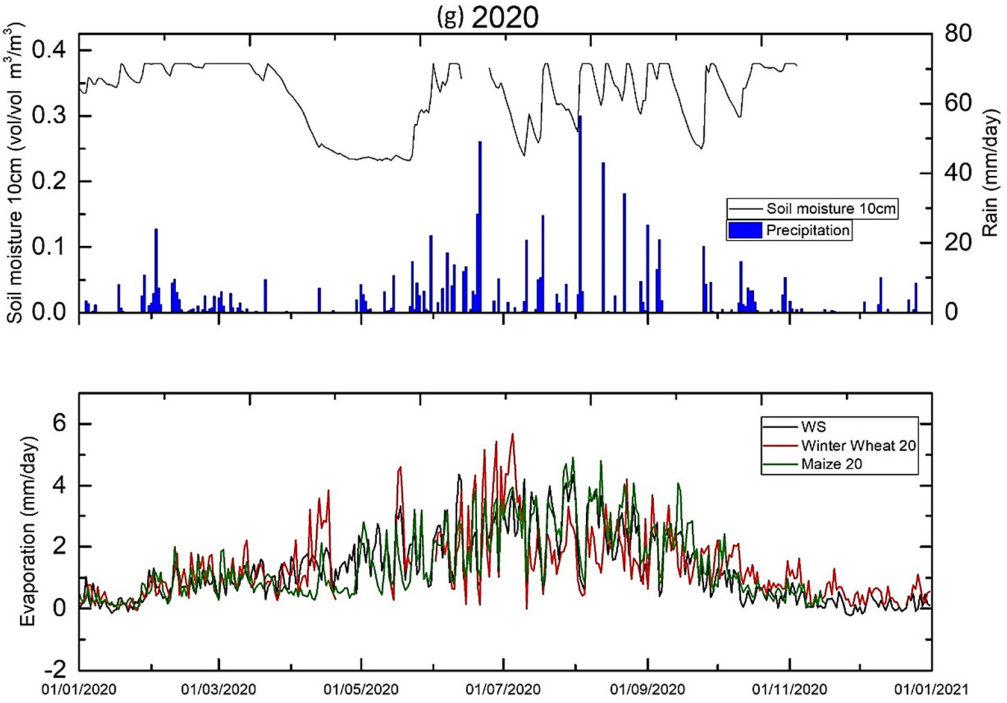

Fig. A1. Daily sums of evaporation at each eddy covariance station, precipitation (blue bars) and soil moisture (black line) 2014–2020.

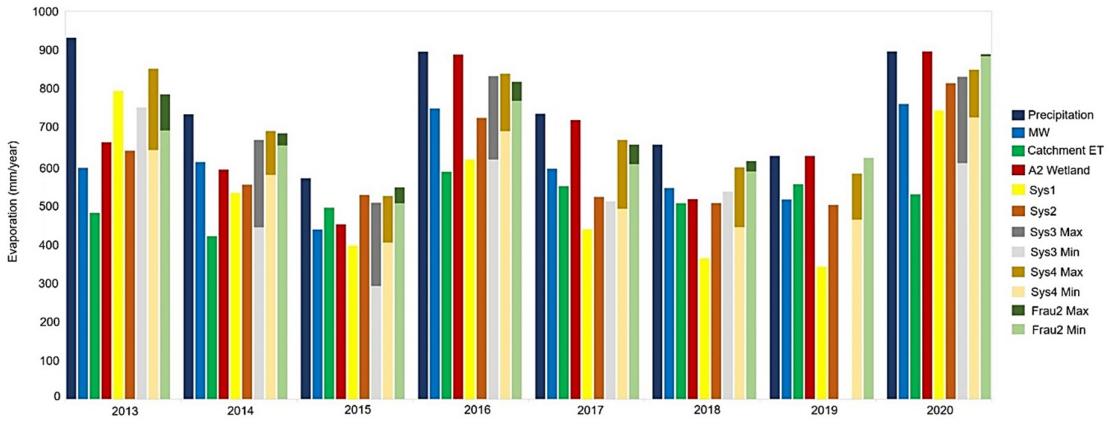

Fig. A2. Comparison of precipitation, catchment average ET and ET + dS calculated from the catchment water balance and subcatchments for 2014–2019.